

Research Paper

Lengthwise Fracture Study of Transversely Inhomogeneous Rods

Victor Iliev RIZOV

*Department of Technical Mechanics
University of Architecture
Civil Engineering and Geodesy*

1 Chr. Smirnensky Blvd., 1046 – Sofia, Bulgaria
e-mail: v_rizov_fhe@uacg.bg

A lengthwise crack in a rod that exhibits smooth (continuous) material inhomogeneity in the transverse direction is studied. The rod has a circular cross-section. The lengthwise crack is located arbitrarily along the thickness of the rod. A solution to the strain energy release rate is derived assuming that the moduli of elasticity in tension and compression are distributed continuously in the transverse direction. The strain energy release rate is also analyzed by applying the compliance method for verification. The influences of various factors such as the crack location, material inhomogeneity and the different mechanical behavior of the material in tension and compression on the fracture are investigated and discussed in detail.

Key words: continuous material inhomogeneity; circular cross-section rod; lengthwise crack.

1. INTRODUCTION

Modern engineering requires extensive use of high performance inhomogeneous structural materials whose mechanical properties depend on coordinates [1, 2]. The inhomogeneous materials, however, are relatively unexplored and, therefore, used with caution. It should be mentioned that the strong interest in inhomogeneous materials is due mainly to the application of functionally graded materials in aerospace, automobile and biomedical applications. Functionally graded materials are advanced composite materials whose composition and microstructure vary gradually along one or more spatial directions [3–8]. The spatial variation of material properties can be tailored during manufacturing process to satisfy specific usage requirements of functionally graded structural members and components.

The fact that the properties of inhomogeneous materials vary continuously with coordinates indicates that more advanced theoretical models and methods

are needed in comparison to these used for analyzing the mechanical behavior of the conventional homogeneous structural materials. The same holds in respect to the models and methodologies which are applied for the analysis of fracture behavior of inhomogeneous materials. The fracture analysis is very important for an adequate assessment of the operational performance of engineering structures. It should also be noted that structural integrity depends to a great extent on the fracture behavior. It is obvious that understanding the fracture behavior is of exceptional importance for improving the design methodology, reducing the cost of eventual repairs and increasing the serviceability of structural members and components made of inhomogeneous materials. Undoubtedly, fracture analysis of inhomogeneous materials and structures is of a significant interest for both academicians and practicing engineers. Therefore, recently, several works on the lengthwise fracture of inhomogeneous (functionally graded) structural members have been published (the interest toward the lengthwise fracture is due to the fact that some inhomogeneous materials such as functionally graded materials can be built-up layer by layer [9], which is a premise for appearance of lengthwise cracks between layers) [10–12]. These works are concentrated mainly on analyzing lengthwise cracks in inhomogeneous beam configurations of rectangular cross-section. Various solutions of the strain energy release rate have been derived assuming that the material is functionally graded along the beam height or the beam height and length [10, 11]. Investigations of lengthwise (delamination) cracks in functionally graded beam structures of circular cross-section loaded in torsion have also been carried out assuming that the material is functionally graded in the radial direction [12].

The main goal of the present paper is to analyze lengthwise fracture in transversely inhomogeneous rods of circular cross-section by applying linear-elastic fracture mechanics methods. The rods are under four-point bending. It is assumed that the rods are made of inhomogeneous material that exhibits different mechanical behavior in tension and compression. The fracture behavior is studied in terms of the strain energy release rate assuming that the moduli of elasticity in tension and compression vary continuously in the rod's transverse direction. The solution to the strain energy release rate derived in the present paper is verified by applying the compliance method. The solution to the strain energy release rate is used to investigate the influence of crack location in the thickness direction, material inhomogeneity and the different mechanical behavior of the material in tension and compression on the fracture behavior.

2. THE SOLUTION FOR THE STRAIN ENERGY RELEASE RATE

An inhomogeneous rod is shown in Fig. 1. The rod has a circular cross-section of radius R_1 (Fig. 2). The length of the rod is $2l + l_1$. The rod exhibits smooth

where U is the strain energy in the beam, Π is the potential of external forces, and dA is an elementary increase of the crack area. Since [14]

$$(2.2) \quad \Pi = -2U,$$

formula (2.1) is rewritten as

$$(2.3) \quad G = \frac{dU}{dA},$$

where the elementary increase of the crack area is expressed as

$$(2.4) \quad dA = b da.$$

In (2.4), da is an elementary increase of the crack length and b is the length of the crack front. Since (Fig. 2)

$$(2.5) \quad b = 2\sqrt{R_1^2 - (R_1 - h_1)^2},$$

formula (2.3) takes the form

$$(2.6) \quad G = \frac{dU}{2\sqrt{R_1^2 - (R_1 - h_1)^2} da}.$$

The strain energy is written as

$$(2.7) \quad U = U_1 + U_2 + U_3,$$

where U_1 , U_2 and U_3 are the strain energies in the upper and lower crack arms in the rod's portion B_2B_3 , and in the uncracked portion B_3B_4 of the rod, respectively. It should be noted that the strain energy in the rod's portions B_1B_2 and B_4B_5 is not involved in (2.7) since this strain energy does not depend on the crack length.

Since the material exhibits different mechanical behavior in tension and compression, the strain energy densities in the tension and compression zones are different. Therefore, the strain energy cumulated in the upper crack arm is written as

$$(2.8) \quad U_1 = (a - l) \iint_{A_c} u_{01c} dA + (a - l) \iint_{A_t} u_{01t} dA,$$

where A_c and A_t are respectively the areas of compression and tension zones in the cross-section of the upper crack arm (Fig. 3). In Eq. (2.8), the strain energy

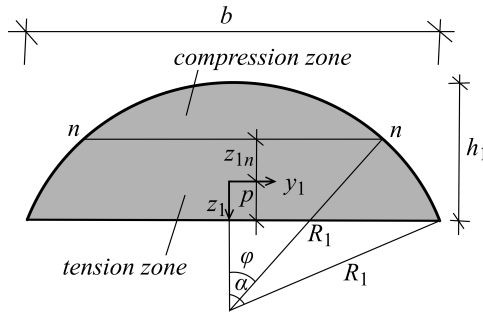


FIG. 3. Cross-section of the upper crack arm (the position of the neutral axis is marked by $n - n$).

densities in the compression and tension zones are denoted by u_{01c} and u_{01t} , respectively.

The strain energy densities in the upper crack arm are obtained as

$$(2.9) \quad u_{01c} = \frac{1}{2} \sigma_c \varepsilon,$$

$$(2.10) \quad u_{01t} = \frac{1}{2} \sigma_t \varepsilon,$$

where σ_c and σ_t are respectively the normal stresses in the compression and tension zones and ε is the longitudinal strain in the upper crack arm. The normal stresses are obtained by the Hooke's law

$$(2.11) \quad \sigma_c = E_c \varepsilon,$$

$$(2.12) \quad \sigma_t = E_t \varepsilon,$$

where E_c and E_t are the moduli of elasticity in the compression and tension zones, respectively. The distributions of E_c and E_t in the transverse direction of the rod are expressed as

$$(2.13) \quad E_c = E_{0c} + \frac{E_{Sc} - E_{0c}}{2R_1} (R_1 + z_4),$$

$$(2.14) \quad E_t = E_{0t} + \frac{E_{St} - E_{0t}}{2R_1} (R_1 + z_4),$$

where

$$(2.15) \quad -R_1 \leq z_4 \leq R_1.$$

In Eq. (2.13), E_{0c} and E_{Sc} are respectively the values of the modulus of elasticity in compression in the upper and lower points of the rod's cross-section,

and z_4 is the vertical centroidal axis (Fig. 2). The values of the modulus of elasticity in tension in the upper and lower points of the rod's cross-section are denoted by E_{0t} and E_{St} , respectively.

The longitudinal strains are analyzed by applying Bernoulli's hypothesis for plane sections since rods with high length to diameter ratio are under consideration in the present paper. Thus, the longitudinal strains are distributed linearly along the height of the upper crack arm

$$(2.16) \quad \varepsilon = \kappa_1(z_1 - z_{1n}),$$

where κ_1 is the curvature of the upper crack arm and z_{1n} is the coordinate of the neutral axis $n - n$ (Fig. 3).

The quantities κ_1 and z_{1n} are determined in the following manner. First, the equations for the equilibrium of the elementary forces in the cross-section of the upper crack arm are written

$$(2.17) \quad N_1 = \iint_{A_c} \sigma_c dA + \iint_{A_t} \sigma_t dA,$$

$$(2.18) \quad M_1 = \iint_{A_c} \sigma_c z dA + \iint_{A_t} \sigma_t z dA,$$

where N_1 and M_1 are the axial force and the bending moment in the upper crack arm, respectively. It is obvious that (Fig. 1)

$$(2.19) \quad N_1 = 0.$$

By substituting (2.11), (2.12) and (2.16) in (2.17) and (2.18) and by using the polar coordinates R and ψ one arrives at

$$(2.20) \quad N_1 = 2 \int_{\frac{\pi}{2}-\alpha}^{\frac{\pi}{2}-\varphi} \int_{R_d}^{R_1} E_t \kappa_1 (z_1 - z_{1n}) R dR d\psi \\ + 2 \int_{\frac{\pi}{2}-\varphi}^{\frac{\pi}{2}} \int_{R_d}^{R_t} E_t \kappa_1 (z_1 - z_{1n}) R dR d\psi + 2 \int_{\frac{\pi}{2}-\varphi}^{\frac{\pi}{2}} \int_{R_t}^{R_1} E_c \kappa_1 (z_1 - z_{1n}) R dR d\psi,$$

$$(2.21) \quad M_1 = 2 \int_{\frac{\pi}{2}-\alpha}^{\frac{\pi}{2}-\varphi} \int_{R_d}^{R_1} E_t \kappa_1 (z_1 - z_{1n}) z_1 R dR d\psi$$

$$+ 2 \int_{\frac{\pi}{2}-\varphi}^{\frac{\pi}{2}} \int_{R_d}^{R_t} E_t \kappa_1 (z_1 - z_{1n}) z_1 R dR d\psi + 2 \int_{\frac{\pi}{2}-\varphi}^{\frac{\pi}{2}} \int_{R_t}^{R_1} E_c \kappa_1 (z_1 - z_{1n}) z_1 R dR d\psi,$$

where

$$(2.22) \quad R_d = \frac{R_1 - h_1}{\sin \psi}, \quad R_t = \frac{R_1 - h_1 + p - z_{1n}}{\sin \psi}, \quad \alpha = \arcsin \frac{b}{2R_1},$$

$$(2.23) \quad \varphi = \arccos \frac{R_1 - h_1 + p - z_{1n}}{R_1}, \quad z_1 = p - [R \sin \psi - (R_1 - h_1)].$$

The angles α and φ are shown in Fig. 3. The following formula is applied to obtain p (Fig. 3) [15]:

$$(2.24) \quad p = \frac{4}{3} \frac{R_1 \sin^3 \alpha}{2\alpha - \sin 2\alpha} - R_1 \cos \alpha.$$

It should be noted that the integrals in (2.20) and (2.21) are multiplied by 2 since z_1 is the axis of symmetry (Fig. 3).

There are three unknowns: z_{1n} , κ_1 and M_1 in Eqs (2.20) and (2.21). To determine z_{1n} , κ_1 , and M_1 , we use the fact that the bending moment M is distributed on both crack arms. Thus, it can be written that

$$(2.25) \quad M = M_1 + M_2,$$

where M_2 is the bending moment in the lower crack arm and M is the bending moment in the rod's portion B_2B_4 . It is obvious that $M = Fl$ (Fig. 1). The curvatures of the two crack arms are identical

$$(2.26) \quad \kappa_2 = \kappa_1,$$

where κ_2 is the curvature of the lower crack arm. Furthermore, the equations for the equilibrium of the elementary forces in the cross-section of the lower crack arm are written as

$$(2.27) \quad N_2 = 2 \int_0^\lambda \int_{R_g}^{R_1} E_t \kappa_2 (z_2 - z_{2n}) R dR d\psi + 2 \int_0^\lambda \int_0^{R_g} E_c \kappa_2 (z_2 - z_{2n}) R dR d\psi$$

$$+ 2 \int_\lambda^\beta \int_0^{R_1} E_c \kappa_2 (z_2 - z_{2n}) R dR d\psi + 2 \int_\beta^\pi \int_0^{R_f} E_c \kappa_2 (z_2 - z_{2n}) R dR d\psi,$$

$$\begin{aligned}
 (2.28) \quad M_2 = & 2 \int_0^\lambda \int_{R_g}^{R_1} E_t \kappa_2 (z_2 - z_{2n}) z_2 R \, dR \, d\psi \\
 & + 2 \int_0^\lambda \int_0^{R_g} E_c \kappa_2 (z_2 - z_{2n}) z_2 R \, dR \, d\psi + 2 \int_\lambda^\beta \int_0^{R_1} E_c \kappa_2 (z_2 - z_{2n}) z_2 R \, dR \, d\psi \\
 & + 2 \int_\beta^\pi \int_0^{R_f} E_c \kappa_2 (z_2 - z_{2n}) z_2 R \, dR \, d\psi.
 \end{aligned}$$

In Eqs (2.27) and (2.28),

$$(2.29) \quad R_g = \frac{q + z_{2n}}{\cos \psi}, \quad R_f = \frac{R_1 - h_1}{\cos(\psi - \frac{\pi}{2})}, \quad \lambda = \arccos \frac{q + z_{2n}}{R_1},$$

$$(2.30) \quad \beta = \pi - \alpha, \quad z_2 = \frac{R}{\cos \psi} - q,$$

where angles λ and β are defined in Fig. 4, and q is written as [15]

$$(2.31) \quad q = \frac{b^3}{12\pi R_1^2 - 6R_1^2(2\alpha - \sin 2\alpha)}.$$

The axial force in the lower crack arm N_2 involved in (2.27) is written as (Fig. 1)

$$(2.32) \quad N_2 = 0.$$

The integrals in (2.27) and (2.28) are multiplied by 2 in view of the symmetry (Fig. 4).

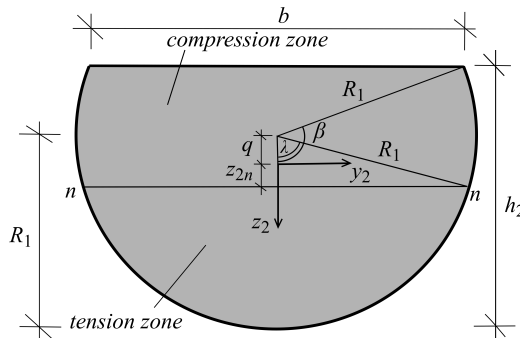


FIG. 4. Cross-section of the lower crack arm (the position of the neutral axis is marked by $n - n$).

After substituting (2.13), (2.14), (2.16), (2.23), (2.23), (2.24), (2.29), (2.30) and (2.31) in (2.20), (2.21), (2.27) and (2.28), the equilibrium equations are solved together with (2.25) and (2.26) with respect to z_{1n} , κ_1 , z_{2n} , κ_2 , M_1 , and M_2 by using the MatLab computer program.

Formula (2.8) is re-written as

$$(2.33) \quad U_1 = 2(a-l) \int_{\frac{\pi}{2}-\alpha}^{\frac{\pi}{2}-\varphi} \int_{R_d}^{R_1} u_{01t} R dR d\psi + 2(a-l) \int_{\frac{\pi}{2}-\varphi}^{\frac{\pi}{2}} \int_{R_d}^{R_t} u_{01t} R dR d\psi + 2(a-l) \int_{\frac{\pi}{2}-\varphi}^{\frac{\pi}{2}} \int_{R_t}^{R_1} u_{01c} R dR d\psi.$$

The strain energy in the lower crack arm is expressed as

$$(2.34) \quad U_2 = 2(a-l) \int_0^\lambda \int_{R_g}^{R_1} u_{02t} R dR d\psi + 2(a-l) \int_0^\lambda \int_0^{R_g} u_{02c} R dR d\psi + 2(a-l) \int_\lambda^\beta \int_0^{R_1} u_{02c} R dR d\psi + 2(a-l) \int_\beta^\pi \int_0^{R_f} u_{02c} R dR d\psi,$$

where u_{02c} and u_{02t} are the strain energy densities in the compression and tension zones of the lower crack arm cross-section, respectively. These strain energy densities are written as

$$(2.35) \quad u_{02c} = \frac{1}{2} E_c [k_2 (z_2 - z_{2n})]^2,$$

$$(2.36) \quad u_{02t} = \frac{1}{2} E_t [k_2 (z_2 - z_{2n})]^2.$$

The strain energy cumulated in the portion B_3B_4 of the rod is written as

$$(2.37) \quad U_3 = 2(l+l_1-a) \left(\int_0^\delta \int_{R_m}^{R_1} u_{03t} R dR d\psi + \int_0^\delta \int_0^{R_m} u_{03c} R dR d\psi + \int_\delta^\pi \int_0^{R_1} u_{03c} R dR d\psi \right),$$

where $R_m = z_{3n}/\cos \delta$ and $\delta = \arccos(z_{3n}/R_1)$. Here, z_{3n} is the neutral axis. The angle δ is shown in Fig. 5. In formula (2.37), u_{03t} and u_{03c} are the strain energy

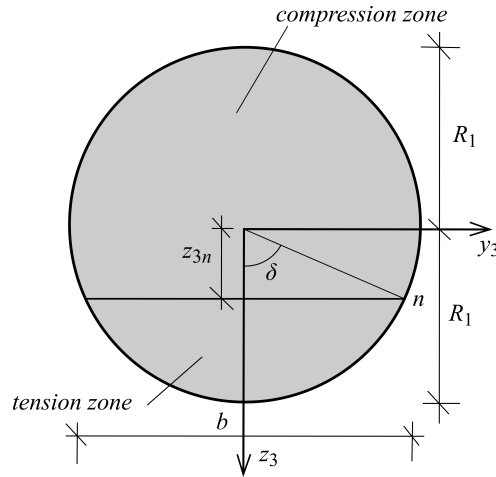


FIG. 5. Cross-section of the rod in the portion, B_3B_4 (the position of the neutral axis is marked by $n-n$).

densities in the tension and compression zones of the cross-section, respectively. The integrals in (2.37) are multiplied by 2 in view of the symmetry.

The following equations for the equilibrium of the elementary forces in the rod's cross-section in the portion B_3B_4 are used to determine κ_3 and z_{3n} :

$$(2.38) \quad N_3 = 2 \int_0^\delta \int_{R_m}^{R_1} E_t \kappa_3 (z_3 - z_{3n}) R dR d\psi \\ + 2 \int_0^\delta \int_0^{R_m} E_c \kappa_3 (z_3 - z_{3n}) R dR d\psi + 2 \int_\delta^\pi \int_0^{R_1} E_c \kappa_3 (z_3 - z_{3n}) R dR d\psi,$$

$$(2.39) \quad M_3 = 2 \int_0^\delta \int_{R_m}^{R_1} E_t \kappa_3 (z_3 - z_{3n}) z_3 R dR d\psi \\ + 2 \int_0^\delta \int_0^{R_m} E_c \kappa_3 (z_3 - z_{3n}) z_3 R dR d\psi + 2 \int_\delta^\pi \int_0^{R_1} E_c \kappa_3 (z_3 - z_{3n}) z_3 R dR d\psi,$$

where the axial force N_3 is zero (Fig. 1), κ_3 is the curvature, and $z_3 = R \cos \psi$.

By substituting U_1 , U_2 , and U_3 in (2.7) and then in (2.6), one obtains the following expression for the strain energy release rate:

$$\begin{aligned}
 (2.40) \quad G = & \frac{1}{\sqrt{R_1^2 - (R_1 - h_1)^2}} \left(\int_{\frac{\pi}{2}-\alpha}^{\frac{\pi}{2}-\varphi} \int_{R_d}^{R_1} u_{01t} R dR d\psi + \int_{\frac{\pi}{2}-\varphi}^{\frac{\pi}{2}} \int_{R_d}^{R_t} u_{01t} R dR d\psi \right. \\
 & + \int_{\frac{\pi}{2}-\varphi}^{\frac{\pi}{2}} \int_{R_t}^{R_1} u_{01c} R dR d\psi + \int_0^\lambda \int_{R_g}^{R_1} u_{02t} R dR d\psi + \int_0^\lambda \int_0^{R_g} u_{02c} R dR d\psi \\
 & + \int_\lambda^\beta \int_0^{R_1} u_{02c} R dR d\psi + \int_\beta^\pi \int_0^{R_f} u_{02c} R dR d\psi \\
 & \left. - \int_0^\delta \int_{R_m}^{R_1} u_{03t} R dR d\psi - \int_0^\delta \int_0^{R_m} u_{03c} R dR d\psi - \int_\delta^\pi \int_0^{R_1} u_{03c} R dR d\psi \right).
 \end{aligned}$$

After substituting (2.9)–(2.14), (2.35) and (2.36) in (2.40), the integration is performed by the MatLab computer program.

The strain energy release rate is also derived by applying the compliance method in order to verify (2.40). According to the compliance method, the strain energy release rate is expressed as

$$(2.41) \quad G = \frac{1}{2} \frac{F^2}{b} \left(\frac{dC_1}{da} + \frac{dC_2}{da} \right),$$

where the compliances, C_1 and C_2 , are written as

$$(2.42) \quad C_1 = \frac{w_1}{F},$$

$$(2.43) \quad C_2 = \frac{w_2}{F}.$$

In (2.42) and (2.43), w_1 and w_2 are the vertical displacements of the rod's cross-sections B_2 and B_4 , respectively (Fig. 1). By applying the integrals of Maxwell-Mohr, one derives

$$\begin{aligned}
 (2.44) \quad w_1 = & \int_0^l \kappa_4 \frac{l+l_1}{2l+l_1} x_4 dx_4 + \int_l^a \kappa_1 \left(\frac{l+l_1}{2l+l_1} x_4 - x_4 + l \right) dx_4 \\
 & + \int_a^{l+l_1} \kappa_3 \left(\frac{l+l_1}{2l+l_1} x_4 - x_4 + l \right) dx_4 + \int_{l+l_1}^{2l+l_1} \kappa_5 \left(\frac{l+l_1}{2l+l_1} x_4 - x_4 + l \right) dx_4,
 \end{aligned}$$

$$(2.45) \quad w_2 = \int_0^l \kappa_4 \frac{l}{2l+l_1} x_4 dx_4 + \int_l^a \kappa_1 \frac{l}{2l+l_1} x_4 dx_4 \\ + \int_a^{l+l_1} \kappa_3 \frac{l}{2l+l_1} x_4 dx_4 + \int_{l+l_1}^{2l+l_1} \kappa_5 \left(\frac{l}{2l+l_1} x_4 - x_4 + l + l_1 \right) dx_4,$$

where x_4 is the longitudinal centroidal axis of the beam, and κ_4 and κ_5 are the curvatures of the rod in the portions B_1B_2 and B_4B_5 , respectively.

After substituting (2.5), (2.42)–(2.44) and (2.45) in (2.41), the strain energy release rate is obtained as

$$(2.46) \quad G = \frac{F}{4\sqrt{R_1^2 - (R_1 - h_1)^2}} \left[(\kappa_1 - \kappa_3) \left(\frac{l+l_1}{2l+l_1} a - a + l \right) \right. \\ \left. + (\kappa_1 - \kappa_3) \frac{l}{2l+l_1} a \right].$$

It should be mentioned that the strain energy release rates calculated by (2.46) are exact matches of these determined by (2.40). This fact proves the correctness of the fracture analysis of inhomogeneous rods with different mechanical behavior of the material in tension and compression presented in this paper.

3. NUMERICAL RESULTS

This section reports numerical results obtained by applying the solution derived in the previous section. Effects of the crack location in the thickness direction, material inhomogeneity and different mechanical behaviour of the material in tension and compression on the lengthwise fracture in the transversely inhomogeneous rod configuration shown in Fig. 1 are investigated. For this purpose, calculations of the strain energy release rate are carried out by applying solution (2.40). The results of these calculations are presented in non-dimensional form by using the formula $G_N = G / (E_{0c}R_1)$. Two ratios of the moduli of elasticity in the upper and the lower points of the cross-section E_{Sc}/E_{0c} are E_{St}/E_{0t} are introduced to characterize the material inhomogeneity in the transverse direction. The ratio $h_1/(2R_1)$ is used in the calculations of the strain energy release rate to characterize the location of the lengthwise crack in the thickness direction. It is assumed that $l = 0.1$ m, $l_1 = 0.20$ m, $R_1 = 0.004$ m, and $F = 2$ N.

The influence of the crack location in the thickness direction on the rod's lengthwise fracture behavior is illustrated in Fig. 6, where the strain energy release rate in non-dimensional form is presented as a function of $h_1/(2R_1)$ ratio at $E_{Sc}/E_{0c} = 0.9$, $E_{0t}/E_{0c} = 0.6$, and $E_{St}/E_{0t} = 1.2$. The curves in Fig. 6

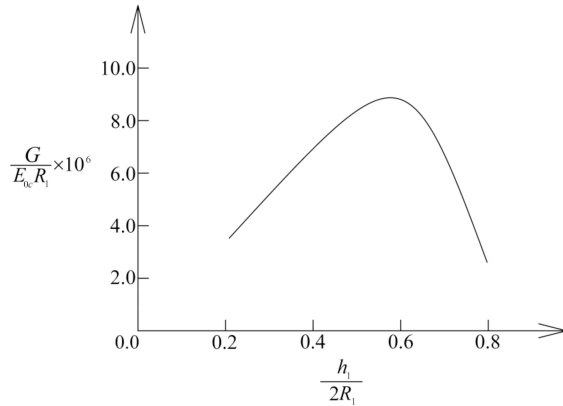


FIG. 6. The strain energy release rate in non-dimensional form presented as a function of $h_1/(2R_1)$ ratio.

indicate that for the considered values of E_{Sc}/E_{0c} , E_{0t}/E_{0c} , and E_{St}/E_{0t} ratios the strain energy release rate gradually increases with increasing $h_1/(2R_1)$ ratio and reaches maximum at $R_2/R_1 = 0.57$. At $R_2/R_1 > 0.57$, the strain energy release rate gradually decreases.

The effect of material inhomogeneity in the transverse direction on the rod's lengthwise fracture behavior is analyzed too. For this purpose, calculations of the strain energy release rate are performed at various E_{Sc}/E_{0c} and E_{St}/E_{0t} ratios. The results obtained are presented as a function of the E_{Sc}/E_{0c} ratio in Fig. 7 at three E_{St}/E_{0t} ratios. In Fig. 7, one can observe that the strain energy release rate decreases with increasing E_{Sc}/E_{0c} ratio. This finding is attributed

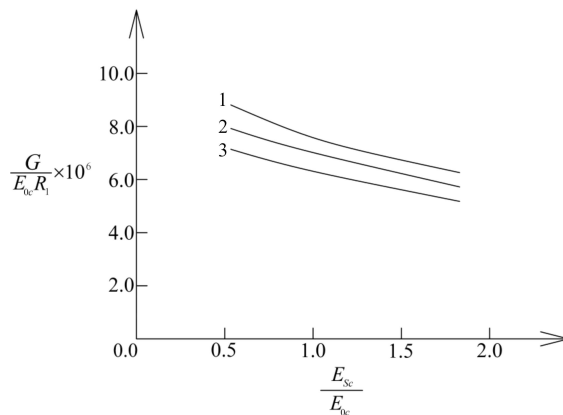


FIG. 7. The strain energy release rate in non-dimensional form presented as a function of E_{Sc}/E_{0c} ratio (curve 1 - at $E_{St}/E_{0t} = 0.5$, curve 2 - at $E_{St}/E_{0t} = 1.5$, and curve 3 - at $E_{St}/E_{0t} = 2.5$).

to the increase of the rod's stiffness with increasing E_{Sc}/E_{0c} ratio. The curves in Fig. 7 also show that the increase of the E_{St}/E_{0t} ratio leads to a decrease in the strain energy release rate.

The dependence of the rod's fracture behavior on the E_{0t}/E_{0c} ratio is also investigated. For this purpose, the strain energy release rate in non-dimensional form is presented as a function of the E_{0t}/E_{0c} ratio in Fig. 8 for two values of the force F . In Fig. 8, it can be observed that the strain energy release rate decreases with increasing of the E_{0t}/E_{0c} ratio. The increase of the force leads to an increase of the strain energy release rate (Fig. 8).

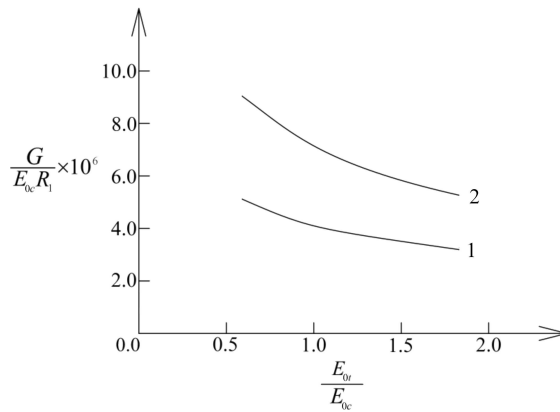


FIG. 8. The strain energy release rate in non-dimensional form presented as a function of E_{0t}/E_{0c} ratio (curve 1 – at $F = 1.5$ N and curve 2 – at $F = 2$ N).

4. CONCLUSIONS

A lengthwise crack in a transversely inhomogeneous rod of a circular cross-section is studied assuming that the material has different mechanical behavior in tension and compression. The rod is loaded in four-point bending. The lengthwise crack is located arbitrarily along the thickness of the rod. Thus, the two crack arms have different thicknesses. The fracture behavior is analyzed in terms of the strain energy release rate assuming that the moduli of elasticity in tension and compression vary continuously in the transverse direction of the rod. A derived solution to the strain energy release rate holds for a crack located arbitrarily in the thickness direction. In order to verify the solution derived, the strain energy release rate is also obtained by applying the compliance method. The two solutions give identical results, what verifies the fracture analysis developed in the present paper. Investigations of the influence of the crack location in the transverse direction, material inhomogeneity and the different mechanical behavior of the material in tension and compression on the fracture are per-

formed. For this purpose, analyses of the strain energy release rate are carried out by using the solution derived. Four ratios: $h_1/(2R_1)$, E_{Sc}/E_{0c} , E_{St}/E_{0t} , and E_{0t}/E_{0c} are introduced in these analyses (the first ratio characterizes the crack location in the thickness direction, the second and the third ratios characterize the material inhomogeneity, while the fourth ratio characterizes the material's different behavior in tension and compression). Concerning the effect of crack location in the thickness direction, it is found that for the considered values of E_{Sc}/E_{0c} , E_{0t}/E_{0c} , and E_{St}/E_{0t} ratios the strain energy release rate gradually increases with increasing $h_1/(2R_1)$ ratio and reaches maximum at $R_2/R_1 = 0.57$. Further increase of $h_1/(2R_1)$ ratio leads to decrease of the strain energy release rate. The analysis shows that the strain energy release rate decreases with increasing of E_{Sc}/E_{0c} and E_{St}/E_{0t} ratios. This finding is attributed to the increase of the rod's stiffness. The investigation reveals that the increase of E_{0t}/E_{0c} ratio also leads to a decrease in the strain energy release rate. From the viewpoint of practical engineering, the results reported in the present paper can be applied in fracture mechanics-based structural design of inhomogeneous members and components. For example, the solution to the strain energy release rate can be used to check for crack growth. For this purpose, the calculated strain energy release rate has to be compared with the critical one. In principle, the critical strain energy release rate known as fracture toughness is determined experimentally by performing mode II lengthwise fracture tests on continuously inhomogeneous beam specimens (the strain energy release rate at the onset of crack growth is the fracture toughness). It should be noted that continuously inhomogeneous beam specimens with initial lengthwise cracks located at various positions along the beam thickness have to be tested. In this way, a fracture toughness profile along the beam thickness will be obtained in contrast to conventional laminate composites for which a single value of the fracture toughness exists.

REFERENCES

1. YASINSKY A., TOKOVA L., Inverse problem on the identification of temperature and thermal stresses in an FGM hollow cylinder by the surface displacements, *Journal of Thermal Stresses*, **40**(12): 1471–1483, 2017, doi: 10.1080/01495739.2017.1357455.
2. TOKOVA L., YASINSKY A., MA C.-C., Effect of the layer inhomogeneity on the distribution of stresses and displacements in an elastic multilayer cylinder, *Acta Mechanica*, **228**: 2865–2877, 2016, doi: 10.1007/s00707-015-1519-8.
3. KOIZUMI M., The concept of FGM, *Ceramic Transactions, Functionally Gradient Materials*, **34**: 3–10, 1993.
4. NEUBRAND A., RÖDEL J., Gradient materials: An overview of a novel concept, *Zeitschrift für Metallkunde*, **88**(5): 358–371, 1997.

5. GASIK M.M., Functionally graded materials: bulk processing techniques, *International Journal of Materials and Product Technology*, **39**(1–2): 20–29, 2010, doi: 10.1504/IJMPT.2010.034257.
6. NEMAT-ALLA M.M., ATA M.H., BAYOUMI M.R., KHAIR-ELDEEN W., Powder metallurgical fabrication and microstructural investigations of aluminum/steel functionally graded material, *Materials Sciences and Applications*, **2**(12): 1708–1718, 2011, doi: 10.4236/msa.2011.212228.
7. BOHIDAR S.K., SHARMA R., MISHRA P.R., Functionally graded materials: A critical review, *International Journal of Research*, **1**(7): 289–301, 2014.
8. AL-HUNITI N.S., ALAHMAD S.T., Transient thermo-mechanical response of a functionally graded beam under the effect of a moving heat source, *Advances in Materials Research*, **6**(1): 27–43, 2017, doi: 10.12989/amr.2017.6.1.027.
9. MAHAMOOD R.M., AKINLABI E., *Functionally graded materials*, Springer, 2017, doi: 10.1007/978-3-319-53756-6.
10. RIZOV V.I., Delamination analysis of a layered elastic-plastic beam, *International Journal of Structural Integrity*, **8**(5): 516–529, 2017.
11. RIZOV V.I., Analysis of delamination in two-dimensional functionally graded multilayered beam with non-linear behaviour of material, *Engineering Transactions*, **66**(1): 61–78, 2018.
12. RIZOV V.I., Non-linear fracture in bi-directional graded shafts in torsion, *Multidiscipline Modeling in Materials and Structures*, **15**(1): 156–169, 2019, doi: 10.1108/MMMS-12-2017-0163.
13. HUTCHINSON J.W., SUO Z., Mixed mode cracking in layered materials, *Advances in Applied Mechanics*, **29**: 63–191, 1991, doi: 10.1016/S0065-2156(08)70164-9.
14. ALEXANDROV A.V., POTAPOV V.D., *Fundamentals of the theory of elasticity and plasticity* [in Russian], Izd-vo “Vyshaya Shkola”, Moscow, 1990.
15. KISSIOV I., *Strength of materials*, Technics, 1995.

Received May 31, 2019; accepted version June 13, 2020.

Published on Creative Common licence CC BY-SA 4.0

